Global phase diagrams for freezing in porous media

Ravi Radhakrishnan
Massachusetts Institute of Technology, Cambridge, Massachusetts 02139

Keith E. Gubbins
North Carolina State University, Raleigh, North Carolina 27695

Malgorzata Sliwinska-Bartkowiak
Institute of Physics, Adam Mickiewicz University, Umultowska 85, 61-614 Poznan, Poland

(Received 23 August 2001; accepted 17 October 2001)

Using molecular simulations and free energy calculations based on Landau theory, we show that freezing/melting behavior of fluids of small molecules in pores of simple geometry can be understood in terms of two main parameters: the pore width H^* (expressed as a multiple of the diameter of the fluid molecule) and a parameter α that measures the ratio of the fluid-wall to the fluid–fluid attractive interaction. The value of the α parameter determines the qualitative nature of the freezing behavior, for example, the direction of change in the freezing temperature and the presence or absence of new phases. For slit-shaped pores, larger α values lead to an increase in the freezing temperature of the confined fluid, and to the presence of a hexatic phase. For pores that accommodate three or more layers of adsorbate molecules several kinds of contact layer phase (inhomogeneous phases in which the contact layer has a different structure than the inner layers) are observed. Smaller α values lead to a decrease in the freezing temperature. The parameter H^* determines the magnitude of shift in the freezing temperature, and can also affect the presence of some of the new phases. Results are presented as plots of transition temperature vs α for a particular pore width. Experimental results are also presented for a variety of adsorbates in activated carbon fibers (ACF) covering a wide range of α values; the ACF have slit-shaped pores with average pore width 1.2 nm. The experimental and simulation results show qualitative agreement. © *2002 American Institute of Physics.* [DOI: 10.1063/1.1426412]

I. INTRODUCTION

Experimental studies of freezing and melting of confined phases within porous media present a complicated and somewhat confusing picture. Such studies must address several difficulties. First is the lack of well-characterized materials having a simple pore geometry, making interpretation difficult. The second difficulty is that of unambiguously determining the nature of the confined phases. The diffraction and scattering experiments commonly used to investigate bulk phases are more difficult to apply to confined phases. A third problem is the prevalence of metastable states, resulting in extensive hysteresis. Molecular simulation studies do not suffer from these difficulties. Although hysteresis is observed, it is possible to calculate free energies of the confined phases, and thus locate true thermodynamic transitions. However, simulations experience other difficulties, particularly uncertainties concerning intermolecular potentials and limitations due to the speed of current computers. The complementary nature of the difficulties in experiment and simulation can make combined experimental-simulation studies in this area rewarding.

Many of the early experimental studies of freezing in porous media[1] employed silica-based materials, and showed a depression of the freezing temperature relative to the bulk fluid ($\Delta T_f = T_{f,\text{pore}} - T_{f,\text{bulk}} < 0$); the lowering of T_f became greater as the pore size decreased. Since these studies employed a range of adsorbates, many scientists concluded that depression of the freezing temperature due to confinement was a general phenomenon. For pore widths much larger than the diameter of the adsorbate molecules the Gibbs–Thomson equation,[1] the freezing analogue of the Kelvin equation for condensation, provides a relation between the shift in the freezing temperature (ΔT_f), the pore width (H) and the surface tensions of the pore wall with the confined fluid (γ_{wl}) and the confined solid (γ_{ws}) phase, and for slit-shaped pores has the form,

$$\frac{\Delta T_f}{T_{f,\text{bulk}}} = -2\frac{(\gamma_{ws} - \gamma_{wl})\nu}{H\lambda_{f,\text{bulk}}}, \tag{1}$$

where ν is the molar volume and $\lambda_{f,\text{bulk}}$ is the latent heat of melting, both for the bulk fluid. Most of the early experiments, which were for pore widths of 5 nm and higher, showed a linear relation between ΔT_f and $1/H$, in accord with Eq. (1). However, the Gibbs–Thomson equation is based on classical thermodynamics, and does not properly account for inhomogeneity of the confined phase or for the adsorbate-wall intermolecular forces. Thus it breaks down for small pores, where the confined phases are highly inhomogeneous.[1]

Miyahara and Gubbins,[2] using Grand Canonical Monte Carlo (GCMC) simulations of the freezing of Lennard-Jones (LJ) methane in slit pores, found that the magnitude and sign of ΔT_f depended on the strength of the adsorbate-wall attractive interaction. For weakly attractive walls, such as silica, ΔT_f was negative, corresponding to a lowering of the freezing temperature on confinement, as found in the experiments.

However, for strongly attractive walls such as carbons ΔT_f was positive, corresponding to an elevation of the freezing temperature. For walls in which the fluid-wall interaction was similar to the fluid–fluid interaction, and the density of wall atoms was similar to the adsorbate density, little or no change in T_f was observed. In this study the freezing and melting temperatures were determined by heating or cooling the sample, and so were the hysteresis temperatures rather than thermodynamic equilibrium ones. However, the findings of Miyahara and Gubbins were later confirmed by simulations in which the free energy of the phases were determined.[3,4] These studies gave the true thermodynamic equilibrium freezing temperatures in the pores, and showed that the transitions were first order in slit pores.

That an elevation of the freezing point might be reasonable for carbons is suggested by the experimental studies of Castro *et al.*,[5] who observed a 10% increase in T_f for the first layer of adsorbed methane and alkanes on a planar graphite substrate. The first experimental observation supporting such an increase in confined systems seems to be that of Klein and Kumacheva,[6] who studied the behavior of cyclohexane confined between parallel mica surfaces in a surface force apparatus. At a pore width of about 4 nm they observed the sudden exhibition of a yield stress, suggesting crystallization. If this interpretation is accepted, the increase in freezing temperature over the bulk material was 17 K. Similar experiments on linear alkanes using the surface force apparatus also show an apparent increase in the freezing temperature relative to the bulk value[7,8] and support for these results comes from a simulation study by Cui *et al.*[9] However, some controversy remains concerning the interpretation of these results; thus, the finding of Klein and Kumacheva[6] for cyclohexane has been disputed by Christenson,[10] who repeated the experiment and found no evidence of an increase in freezing temperature for this system.

More recently, a number of studies for adsorbates confined within activated carbon fibers have shown evidence of an increase in freezing temperature. These materials have approximately slit-shaped pores, and can be prepared with pore widths from 0.7 to about 2 nm. Using differential scanning calorimetry (DSC), Kaneko and co-workers[11,12] found evidence of a large increase in the freezing temperature for both carbon tetrachloride and benzene in these carbons. The elevations in freezing temperature were 57 and 65 K, respectively, for a mean pore width of 1.1 nm. Using both DSC and dielectric relaxation spectroscopy, Sliwinska-Bartkowiak and co-workers have studied the freezing of water,[13] methanol,[13] nitrobenzene,[14] aniline[15] and carbon tetrachloride[16] in activated carbon fibers, and observed a range of freezing behavior. For water, a significant decrease in the freezing temperature was observed, while for nitrobenzene T_f was almost unchanged. For aniline a melting temperature of 298 K was observed, 31 K above the bulk melting temperature of 267 K, for methanol a melting temperature increase of 43 K was observed, while for CCl_4 the results agreed with those of Kaneko *et al.*,[11] the freezing temperature for the confined system being about 57 K above the bulk value. We note that the reduced dipole moment $[\mu^* = \mu/\sqrt{(\epsilon\sigma^3)}$, see Table II] of these adsorbate molecules decreases in the order $H_2O > C_6H_5NO_2 > CH_3OH > C_6H_5NH_2 > CCl_4$.

Many authors[17–24] have reported experimental evidence that the adsorbed molecular layers adjacent to the pore wall have a different structure than that of the inner adsorbed layers. These studies have been for silica materials, and seem to indicate a fluid layer of adsorbate near the walls, while the internal adsorbate layers are solid or crystalline. Some recent DSC and dielectric relaxation studies[13,15,16] of phases confined within slit-shaped carbon pores, for which strong layering of the adsorbate occurs, suggest that a hexatic phase may occur as an intermediary phase between the fluid and crystalline ones. Hexatic phases, which retain long-range orientational, but not positional, order are known to occur in quasi-two-dimensional systems. For cylindrical pores, such as those in MCM-41 and controlled pore glasses, it is found[24–27] that for pore diameters below about 20σ, where σ is the diameter of the adsorbate molecule, the fluid partially crystallizes into a mixture of defective crystal and amorphous regions, and for diameters below about 15σ only amorphous regions are observed. These results are in agreement with molecular simulation results for cylindrical pores in this size range.[24]

In this study, we show that the apparently diverse and complex freezing behavior for small molecules in pores can be classified and understood in terms of two predominant parameters: (1) the relative strength of the fluid-wall to the fluid–fluid attractive interaction, α, and (2) the reduced pore width, $H^* = H/\sigma_{ff}$, where σ_{ff} is the LJ diameter for the adsorbate–adsorbate interaction. By carrying out molecular simulations, together with rigorous free energy calculations based on Landau theory, we are able to present global phase diagrams for slit pores in terms of α and H^*. We further show that the simulation results are in qualitative agreement with existing experimental measurements for activated carbon fibers and mica slit pores. The molecular models and simulation methods are described in Secs. II and III, and the results are presented and discussed in Sec. IV.

II. MODELS AND SIMULATION METHODS

We perform Grand Canonical Monte Carlo (GCMC) simulations of a fluid adsorbed in slit-shaped pores of width H, where H is defined as the perpendicular distance between the planes passing through the nuclei of the first layer of molecules that make up the pore walls of the slit-shaped pore. The interaction between the adsorbed fluid molecules is modeled using the Lennard-Jones (12,6) potential with size and energy parameters, σ_{ff}, ϵ_{ff}. The Lennard-Jones potential was cut off at a distance of $5\sigma_{ff}$, beyond which it was assumed to be zero. The pore walls are modeled as a continuum of LJ molecules using the "10-4-3" Steele potential,[28] given by

$$\phi_{fw}(z) = 2\pi\rho_w\epsilon_{fw}\sigma_{fw}^2\Delta\left[\frac{2}{5}\left(\frac{\sigma_{fw}}{z}\right)^{10} - \left(\frac{\sigma_{fw}}{z}\right)^4 - \left(\frac{\sigma_{fw}^4}{3\Delta(z+0.61\Delta)^3}\right)\right]. \quad (2)$$

TABLE I. Potential energy parameters for fluid–fluid interactions.

Fluid	LJ parameters σ_{ff}/nm, $\epsilon_{ff}/(k_B K)$	Property fitted
Simple fluids		
C_6H_6	0.6, 401.0	Freezing point
C_6H_{12}	0.5, 412.0	Freezing point
CCl_4	0.514, 366.0	Freezing point
CH_4	0.381, 148.1	2nd Virial Coefficient
Dipolar fluids		
$C_6H_5NO_2$	0.514, 425.0	Freezing point
$C_6H_5NH_2$	0.514, 395.0	Freezing point
CH_3OH	0.45, 256.0	Freezing point
H-Bonding fluids		
H_2O	0.3154, 401.0	Freezing point

Here, the σ's and ϵ's are the size and energy parameters in the Lennard-Jones (LJ) potential, the subscripts f and w denote fluid and wall, respectively, Δ is the distance between two successive lattice planes of pore wall, z is the coordinate perpendicular to the pore walls and ρ_w is the number density of the wall atoms. For a given pore width, H, the total potential energy from both walls is given by,

$$\phi_{\text{pore}}(z) = \phi_{fw}(z) + \phi_{fw}(H-z). \tag{3}$$

The strength of attraction of the pore walls relative to the fluid–fluid interaction is determined by the coefficient

$$\alpha = \frac{\rho_w \epsilon_{fw} \sigma_{fw}^2 \Delta}{\epsilon_{ff}} \tag{4}$$

in Eq. (2). Throughout the study three different fluid–fluid interaction parameters were used (see Table I): (1) LJ methane with $\sigma_{ff}=0.381$ nm, $\epsilon_{ff}/k_B=148.1$ K; (2) LJ CCl_4 with $\sigma_{ff}=0.514$ nm, $\epsilon_{ff}/k_B=366$ K; (3) LJ aniline with $\sigma_{ff}=0.514$ nm, $\epsilon_{ff}/k_B=395$ K. Eight different sets of parameters were chosen for the pore wall interaction. This was achieved by fixing $\sigma_{ww}=0.34$ nm and $\Delta=0.335$ nm, the size corresponding to graphitic pores,[28] and letting the product of $\rho_w \times \epsilon_{fw}$ vary over a range, resulting in eight different alpha values, from a purely repulsive wall to a strongly attractive wall ($\alpha=0$ to $\alpha=2.14$). For example, $\alpha=2.14$ corresponds to LJ methane in activated carbon fibers, for which $\rho_w=114$ nm^{-3} and $\epsilon_{ww}/k_B=28$ K. The Lorentz–Berthlot mixing rules, together with the ff and ww parameters, were used to determine the values of σ_{fw} and ϵ_{fw}. The simulation runs were performed by fixing the chemical potential, μ, the volume, V, of the pore and the temperature, T. Two different pore widths, $H=3\sigma_{ff}$ and $H=7.5\sigma_{ff}$ were chosen for study. A rectilinear cell of dimensions $(60\sigma_{ff}\times 60\sigma_{ff})$ in the plane parallel to the pore walls was used. Typically the system consisted of up to 12 000 adsorbed fluid molecules. The adsorbed molecules formed distinct molecular layers parallel to the plane of the pore walls. The simulation was set up such that insertion, deletion and displacement moves were chosen at random with equal probability. Thermodynamic properties were averaged over 2000 million individual Monte Carlo steps.

III. FREE ENERGY DETERMINATION

We extend the Landau free energy approach used in earlier studies[4,29,30] to incorporate *spatial inhomogeneity* in the order parameter, and develop the generalized Landau–Ginzburg approach to calculate the free energy surface of inhomogeneous fluids. The Landau–Ginzburg formalism involves choosing an order parameter Φ, that is sensitive to the degree of order in the system. For the general case of a spatially varying order parameter $\Phi(\mathbf{r})$, the probability distribution function of the order parameter $P[\tilde{\Phi}(\mathbf{r})]$ is defined as

$$P[\tilde{\Phi}(\mathbf{r})] = \frac{1}{\Xi} \sum_{N=1}^{\infty} \frac{\exp(\beta\mu N)}{N!\lambda^{3N}} \int D_N[\Phi(\mathbf{r})] \times \delta(\tilde{\Phi}(\mathbf{r}) - \Phi(\mathbf{r})) \exp(-\beta H_N), \tag{5}$$

where Ξ is the partition function in the grand canonical ensemble, N the number of molecules in the system, $\beta = 1/k_B T$, λ is the de Broglie wavelength, and H_N is the configurational Hamiltonian of the system. The path integral notation, $D_N[\Phi(\tilde{\mathbf{r}})]$, should be interpreted as[31]

$$\int D_N[\Phi(\mathbf{r})] \equiv \lim_{v_o \to 0} \Pi_\alpha \int d\Phi_\alpha = \int_{\mathbf{r}^N} d\mathbf{r}^N. \tag{6}$$

Equation (6) defines the path integral in terms of a trace over a discrete number of sites α, and v_o represents the volume per site. The Landau free energy $\Lambda[\tilde{\Phi}(\mathbf{r})]$ is defined by

$$\exp(-\beta\Lambda[\tilde{\Phi}(\mathbf{r})]) = \sum_{N=1}^{\infty} \frac{\exp(\beta\mu N)}{N!\lambda^{3N}} \int D_N[\Phi(\mathbf{r})] \times \delta(\tilde{\Phi}(\mathbf{r}) - \Phi(\mathbf{r})) \exp(-\beta H_N) \tag{7}$$

so that, from Eq. (5)

$$\Lambda[\Phi(\mathbf{r})] = -k_B T \ln(P[\Phi(\mathbf{r})]) + \text{Constant}. \tag{8}$$

The Landau free energy can be computed by a histogram method combined with umbrella sampling that calculates the probability distribution of the system in the order parameter space. The probability distribution function $P[\Phi(\mathbf{r})]$ is calculated during a simulation run by collecting statistics of the number of occurrences of a particular value of the function $\Phi(\mathbf{r})$. This is accomplished by constructing a histogram with respect to Φ values in different domains obtained by discretizing the spatial coordinates. The procedure to collect statistics, construct the histograms and the choice of weighting functions for performing the umbrella sampling are described in Refs. 4 and 30. The grand free energy of a particular phase A, $\Omega_A = -k_B T \ln(\Xi)$, is then related to the Landau free energy by

$$\exp(-\beta\Omega) = \int D_N[\Phi(\mathbf{r})] \exp(-\beta\Lambda[\Phi(\mathbf{r})]), \tag{9}$$

where the limits of integration in Eq. (9) are from the minimum value of $\Phi(\mathbf{r})$ to the maximum value of $\Phi(\mathbf{r})$ that characterizes the phase A. We use a two-dimensional bond

orientational order parameter to characterize the orientational order in each of the molecular layers that is defined as follows:

$$\Psi_{6,j}(\boldsymbol{\rho}) = \frac{1}{N_b} \sum_{k=1}^{N_b} \exp(i6\theta_k). \tag{10}$$

$\Psi_{6,j}(\boldsymbol{\rho})$ measures the hexagonal bond order at position $\boldsymbol{\rho}$ in the xy plane within each layer j, and is calculated as follows. Nearest neighbors were identified as those particles that were less than a cutoff distance r_{nn} away from a given particle, and belonged to the same layer. We used a cutoff distance $r_{nn}=1.3\sigma_{ff}$, corresponding to the first minimum of $g(r)$. The orientation of the nearest neighbor bond is measured by the θ coordinate, which is the angle the projection of the nearest-neighbor vector on the xy-plane, makes with the x axis. $\Psi_{6,j}(\boldsymbol{\rho})$, is calculated using Eq. (10), where the index k runs over the total number of nearest-neighbor bonds N_b at position $\boldsymbol{\rho}$ in layer j. The order parameter $\Psi_{6,j}$ in layer j is given by $\Psi_{6,j}=|\int d\boldsymbol{\rho}\Psi_{6,j}(\boldsymbol{\rho})|/\int d\boldsymbol{\rho}$. For the case of LJ CCl_4 in slit-shaped pores, where there is significant ordering into distinct molecular layers, the order parameter $\Phi(\mathbf{r})$ can be reduced to $\Phi(z)$ and can be represented by

$$\Phi(z) = \sum_{j=1}^{n} \Psi_{6,j}\,\delta(z-\hat{z}_j). \tag{11}$$

In Eq. (11), the sum is over the number of adsorbed molecular layers and $\hat{z}_j$ is the z coordinate of the plane in which the coordinates of the center of mass of the adsorbed molecules in layer j are most likely to lie on. It must be recognized that each of the $\Psi_{6,j}$'s are variables that can take values in the range $[0,1]$. The histograms can be collected to evaluate the probability $P[\Psi_{6,1},\Psi_{6,2},\ldots,,\Psi_{6,n}]$ as a function of the order parameters $\Psi_{6,1},\Psi_{6,2},\ldots,\Psi_{6,n}$. The grand free energy is then calculated using the equation

$$\exp(-\beta\Omega) = \Pi_{j=1}^{n} \int_j d\Psi_{6,j} P[\Psi_{6,1},\Psi_{6,2}\ldots,,\Psi_{6,n}]. \tag{12}$$

IV. RESULTS

The state conditions in the simulations were chosen such that the confined phase was in equilibrium with the bulk phase at 1 atm pressure. For each set of values of the LJ fluid–fluid interaction and α, the simulations were started from a well equilibrated confined liquid phase, and in successive simulation runs, the temperature was reduced. The two-dimensional, in-plane positional and orientational pair correlation functions [$g_j(r)$ and $G_{6,j}(r)$ of layer j], were monitored to keep track of the nature of the confined phase. The positional pair correlation function is the familiar radial distribution function. The orientational pair correlation function is given by $G_{6,j}(\rho)=\langle\Psi^*_{6,j}(0)\Psi_{6,j}(\rho)\rangle$. The Landau–Ginzburg free energy calculations were then performed to locate the phase transitions in state space.

We illustrate the above scheme for LJ CCl_4 confined in activated carbon fibers of pore width, $H^*=3$. Our results for the positional and orientational pair correlation functions for the two confined molecular layers of LJ CCl_4 at three different temperatures are given in Fig. 1. It is evident from Fig. 1 that the high temperature phase at $T=360$ K, with an isotropic $g(r)$ and exponentially decaying $G_{6,j}(r)$, is a dense fluid (liquid) phase with short-range positional order and short-ranged orientational order. The confined phase at $T=340$ K is characterized by an isotropic positional pair correlation function and an algebraically decaying orientational correlation function; this is a clear signature of the hexatic phase with short-range positional order and quasi-long-ranged orientational order. At $T=290$ K the confined phase is a two-dimensional hexagonal crystal, with quasi-long-range positional order and long-range orientational order.

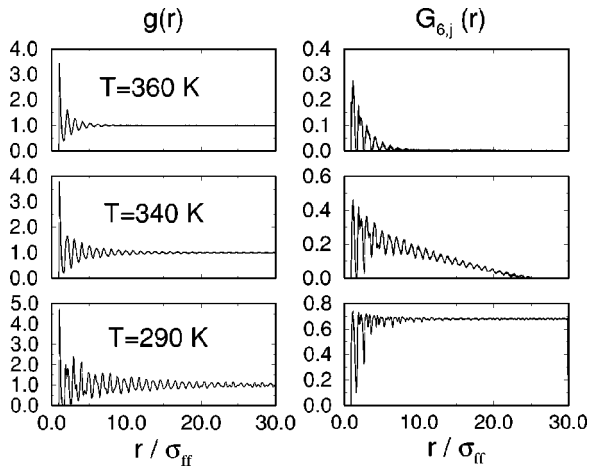

FIG. 1. $g(r)$ and $G_6(r)$ in the two molecular layers of CCl_4 confined in a graphite pore of width $H=3\sigma_{ff}$ ($\alpha=1.92$): (a) liquid ("L") phase at $T=360$ K; (b) hexatic ("H") phase at $T=340$ K; (c) crystalline ("C") phase at $T=290$ K.

Two-dimensional systems have a special significance for phase transitions in which continuous symmetry is broken, such as freezing transitions. The Mermin–Wagner theorem states that true long-range order cannot exist in such systems.[32] Nelson and Halperin[33] proposed the "KTHNY" (Kosterlitz–Thouless–Halperin–Nelson–Young) mechanism for melting of a crystal in two dimensions which involves two transitions of the Kosterlitz–Thouless (KT) kind:[34] the first is a transition between the two-dimensional crystal phase (with quasi-long-range positional order and long range orientational order) and a hexatic phase (with positional disorder and quasi-long-range orientational order); the second transition is between the hexatic phase and the liquid phase (having positional and orientational disorder). Each KT transition is accompanied by a nonuniversal peak in the specific heat above the transition temperature, associated with the entropy liberated by the unbinding of the vortex pairs. The crystal to hexatic transition occurs through the unbinding of dislocation pairs, and the hexatic to liquid transition involves the unbinding of disclination pairs.

For the pore width, $H^*=3$, the Landau free energy surface is a function of two variables (there are two confined layers in the system), $\Lambda/k_BT=\Lambda[\Psi_{6,1},\Psi_{6,2}]/k_BT$. This function was calculated at two different temperatures, $T=335$ K and $T=290$ K, from which the grand free energies

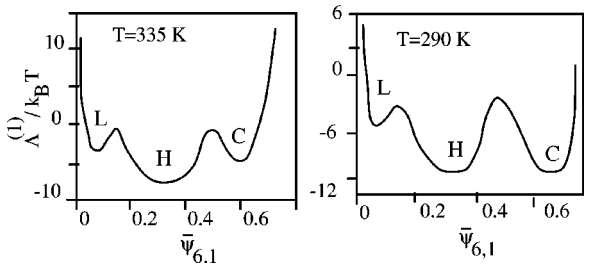

FIG. 2. The first order distribution functions of the Landau free energy for layer 1 at $T=335$ K and $T=290$ K, for LJ CCl_4 in a graphite pore, $H^*=3$.

of the liquid (L), hexatic (H) and crystal (C) phases at these different temperatures were calculated using Eq. (12). The grand free energy of the three phases at other temperatures were further calculated using thermodynamic integration,[35] using the temperatures $T=335$ K and $T=290$ K as reference. The first order distribution function of the Landau free energy functions for the first molecular layer (layer 1), $\Lambda^{(1)}\times[\Psi_{6,1}]$ [which is obtained by the taking the functional derivative of Eq. (12) with respect to the order parameter $\Psi_{6,1}$ in layer 1], at $T=335$ K and $T=290$ K are shown in Fig. 2.

The distribution functions in Fig. 2 are good representations of the three-dimensional Landau free energy surface for the system considered here because the fluid-wall potential energy is symmetric with respect to the two confined molecular layers of CCl_4, causing the matrix $\Lambda[\Psi_{6,1},\Psi_{6,2}]$ to be symmetric. Further, the lowest free energy state points that govern the equilibrium thermodynamics of the system are given by the diagonal elements and the elements near the diagonal of the matrix.

The presence of the three phases ("L," "H," and "C") of the system is clearly seen in Fig. 2, along with their relative thermodynamic stabilities; the nature of these phases were determined from the positional and orientational correlation functions (Fig. 1). It is clear from Fig. 2 that the hexatic phase is the thermodynamically stable phase at $T=335$ K, while $T=290$ K is close to the temperature at which the hexatic and crystalline phases coexist. The grand free energy function for the three phases ("L," "H," and "C") are given in Fig. 3. The crossover of the free energy functions at $T=347$ K and $T=290$ K provide the transition temperatures of the liquid-hexatic and the hexatic-crystal transitions. The crossover of the free energy of the different phases at different slopes at the transition temperatures implies that both transitions are first order, at least for this particular system size.

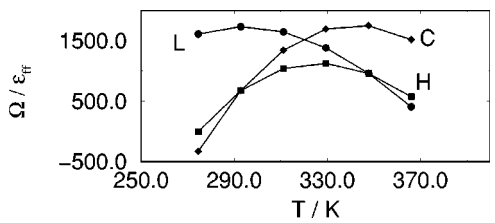

FIG. 3. The Grand free energy as a function of temperature for liquid, hexatic and crystalline phases, for LJ CCl_4 in a graphite pore, $H^*=3$.

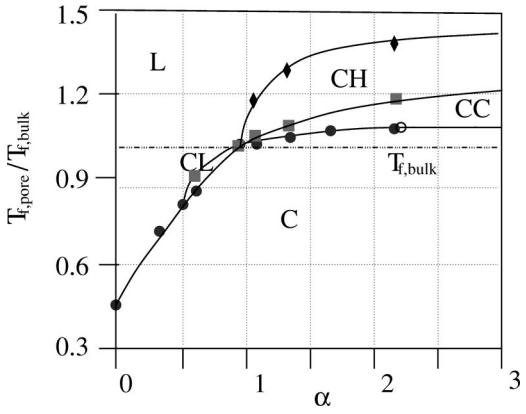

FIG. 4. Global freezing phase diagram for a Lennard-Jones fluid in a slit-shaped pore of width $H=7.5\sigma_{ff}$ and a bulk pressure of 1 atm. The symbols (filled diamonds, filled circles and filled squares in present figure) specify the conditions of co-existence of two phases, obtained using Landau free energy calculations. The solid lines passing through the symbols are a guide to the eye and represent the phase boundaries separating the different phases. Five different phases are observed: liquid, contact-hexatic, contact-crystal, contact-liquid and crystalline. The different phases are characterized by the positional and orientational correlation functions as depicted in Figs. 5–9. The "dash-dot-dot-dot" line represents the freezing temperature of a LJ fluid under ambient pressures and is provided for reference. The point marked by the open circle is the experimental result of Klein and Kumacheva (Ref. 6) for cyclohexane in a mica slit pore.

In a previous study[14] we used corresponding states theory to show that the freezing temperature of the confined fluid relative to that of the bulk fluid was a function of the dimensionless parameters H^*,α, and the diameter ratio σ_{fw}/σ_{ff}. However, the freezing temperature ratio was found to be only very weakly dependent on the diameter ratio, provided the diameters were not very different and the pore size did not closely approach the molecular sieving regime. Here we show that the global freezing behavior, i.e., other transitions associated with the liquid to crystalline change, in addition to the freezing temperature, obeys such a corresponding states argument, and so is governed by the variables H^* and α; the diameter ratio again plays a minor role, subject to the caveats above. This corresponding states principle states that the phase behavior for two different adsorbates in two different materials will be (approximately) the same if they have the same values of H^* and α. Thus, the construction of phase diagrams from a minimum of simulation or experimental data, provided they cover a suitably wide range of H^* and α values, can be used to predict the phase behavior of other systems that have not been studied. In what follows we present such global phase diagrams for a range of realistic values of α. In addition to varying α in our simulations, we also carry out calculations for two different values of σ_{fw}/σ_{ff}, corresponding to methane and carbon tetrachloride in graphite pores, and thus show that the phase behavior is almost independent of the diameter ratio for the range studied (σ_{ff} values from 0.38 to 0.51 nm).

Global phase diagrams for two different pore widths were constructed by spanning the parameter space in α and $T_{f,\mathrm{pore}}/T_{f,\mathrm{bulk}}$, maintaining a pressure of 1 atm. A summary of the phase behavior of a Lennard-Jones fluid in slit-shaped pores of width $H=7.5\sigma_{ff}$ is given in Fig. 4. For this system

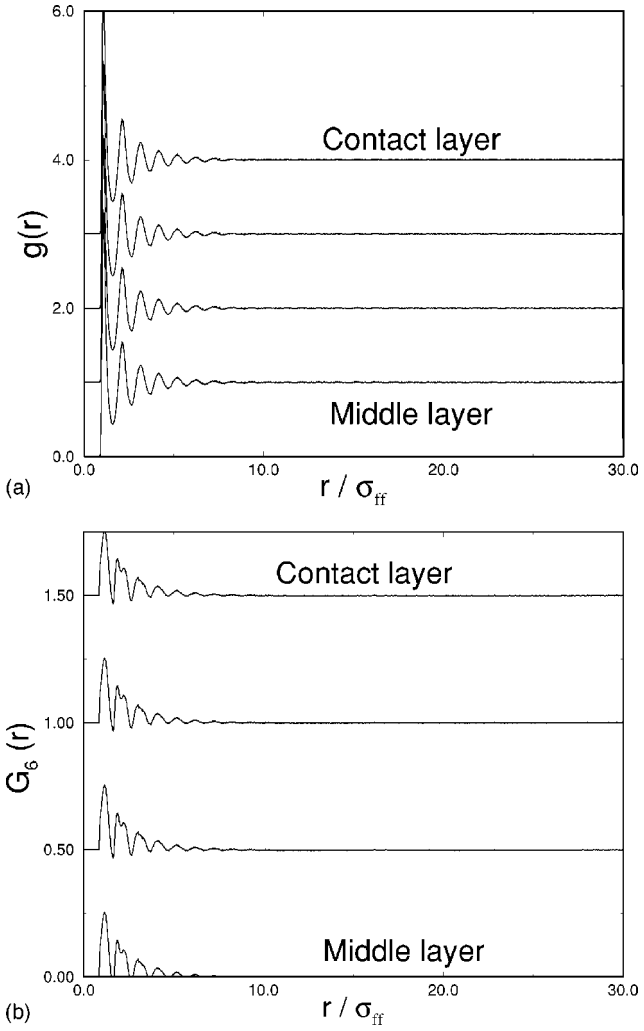

FIG. 5. The 2D in-plane (a) positional and (b) orientational pair correlation functions in the confined molecular layers for a LJ fluid in a slit-shaped pore of width $H=7.5\sigma_{ff}$ for $\alpha=2.16$, $T^*=1.02$: liquid phase. The zero of $g(r)$ has been shifted on the vertical scale for layers other than the middle layer, for clarity.

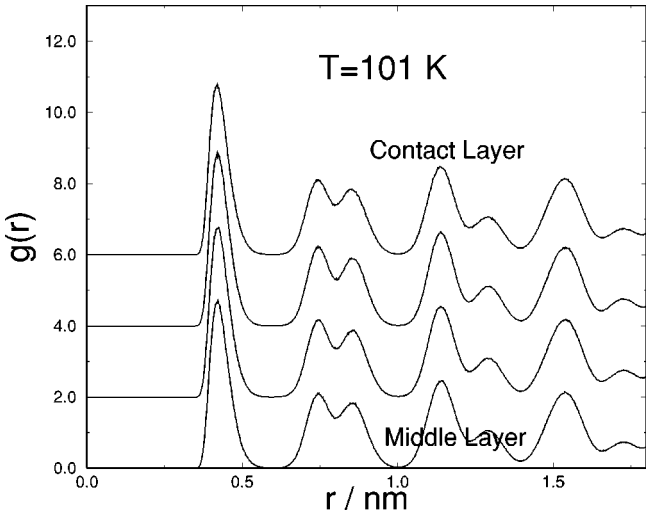

FIG. 6. The 2D in-plane positional correlation functions in the confined molecular layers for a LJ fluid in a slit-shaped pore of width $H=7.5\sigma_{ff}$ for $\alpha=2.16$, $T^*=0.61$: crystalline phase.

the Landau free energy is a function of seven variables, as there are seven confined layers in the pore, $\Lambda/k_BT=\Lambda[\Psi_{6,1},\Psi_{6,2},\ldots,\Psi_{6,7}]/k_BT$. This function was calculated at three different temperatures, for eight different values of α. For a given value of α, the grand free energies were calculated for each phase at three different temperatures using Eq. (12). Grand free energies at intermediate temperatures were then computed using thermodynamic integration.[4] For a given α, the condition for phase coexistence was determined by identifying the temperature at which the grand free energies of the corresponding phases were equal. The phase diagram obtained using this procedure is depicted in Fig. 4. The reduced freezing temperature of the bulk Lennard-Jones fluid (with the LJ potential cutoff at $3\sigma_{ff}$, and long-range correction applied), at 1 atm pressure, is $T^*=0.682$,[36,37] and is depicted by $T_{f,\mathrm{pore}}/T_{f,\mathrm{bulk}}=1$, the horizontal ''dash-dot-dot-dot'' line in Fig. 4. In the case of the confined system, the crystal phase boundary is marked by the circles, below which the crystalline (C) phase is stable. The freezing temperature of the confined phase (given by the solid circles) shifts upward on confinement for values of α greater than 0.95 (strongly attractive pores), and shifts downward for values of α less than 0.95 (weakly attractive pores).

In Fig. 4, the solid squares represent the freezing temperature of a ''partially crystalline phase;'' the contact layers (layers adjacent to the pore walls) freeze (become crystalline) at a different temperature than the inner layers. For strongly attractive pores, the contact layers freeze at a temperature higher than the inner layers, while for weakly attractive walls the contact layers freeze at a temperature lower than the inner layers; this leads to the formation of two new phases that we term *contact-crystalline* (CC) and *contact-liquid* (CL) phases, respectively. The contact-crystalline phase is thermodynamically stable in the region $\alpha>0.95$, between the squares and the circles. The contact-liquid phase is a stable phase in the region $\alpha<0.95$, between the squares and the circles. For strongly attractive pores, $\alpha>0.95$, the contact layers undergo a second, liquid-hexatic phase transition (shown as solid diamonds), that leads to the formation of another new phase that we term *contact-hexatic* (CH).[38] The stable regions of the contact-hexatic phase are between the lines marked by the diamonds and the squares in Fig. 4.

The only experimental data we are aware of for freezing of a fluid of small molecules in a slit-shaped pore of this pore width are those of Klein and Kumacheva[6] for cyclohexane in a mica pore. Based on the reported freezing temperature for this system and the mica potential parameters of Cui *et al.*[9] (see Table III), we find $T_{f,\mathrm{pore}}/T_{f,\mathrm{bulk}}=1.055$ and $\alpha=2.22$. This point is in excellent agreement with the simulation results shown for the freezing transition (Fig. 4), the freezing temperature being about 6% above that for the bulk fluid. However, as noted in Sec. I, there is still some controversy associated with the nature of the shift in the freezing point for cyclohexane in mica, so that this result should be treated with some caution. In addition, the value given for the parameter ϵ_{ww}/k_B for mica of 940 K by Cui *et al.*[9] may be somewhat uncertain.[39] However, a significant change in this parameter (and hence in the value for α) would not signifi-

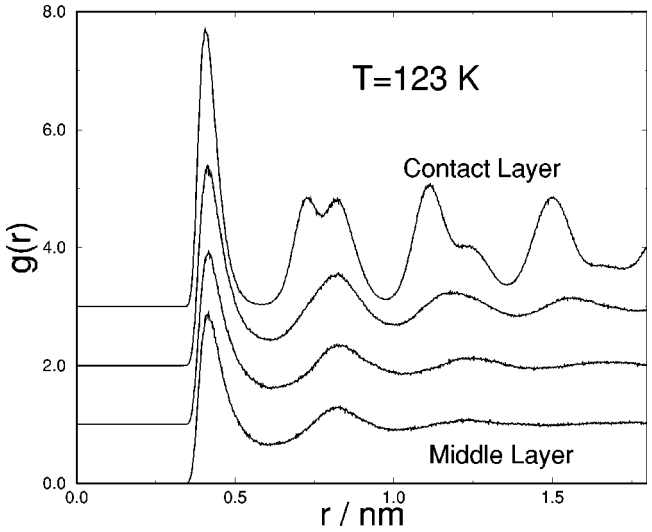

FIG. 7. The 2D in-plane positional correlation functions in the confined molecular layers for a LJ fluid in a slit-shaped pore of width $H=7.5\sigma_{ff}$ for $\alpha=2.16$, $T^*=0.75$: contact-crystalline phase.

cantly affect the agreement with simulation shown in Fig. 4, since the freezing curve is almost flat in the range $1.5<\alpha<3$.

While the co-existence curves from simulation are obtained from the grand free energies, the nature of the different phases is distinguished on the basis of the behavior of the two-dimensional, in-plane pair correlation function, $g(r)$, and the orientational correlation function, $G_{6,j}(\rho)$, in the confined molecular layers. Examples are shown in Figs. 5–9. The pair correlation functions in the liquid phase are isotropic [Fig. 5(a)] and those in the crystalline phase correspond to a 2-D hexagonal crystal [Fig. 6], in each of the confined layers. In addition, the behavior of the orientational correlation functions in the liquid phase show an exponential decay [Fig. 5(b)]. The contact-crystalline phase consists of a crystalline contact layer and liquid-like inner layers (Fig. 7),

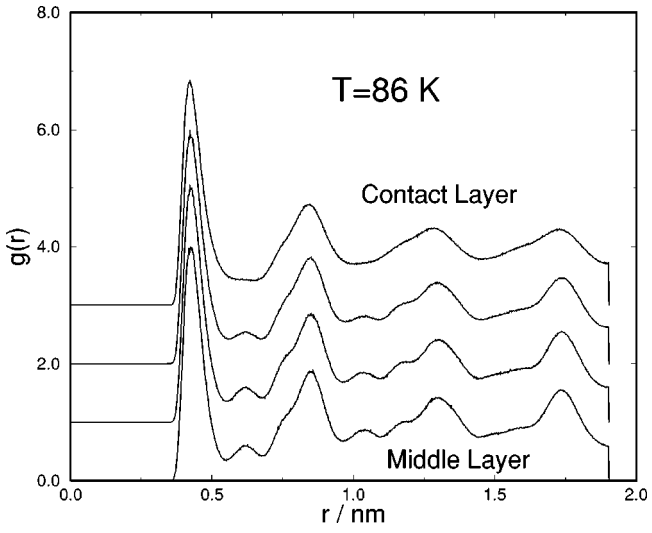

FIG. 8. The 2D in-plane positional correlation functions in the confined molecular layers for a LJ fluid in a slit-shaped pore of width $H=7.5\sigma_{ff}$ for $\alpha=0.62$, $T^*=0.61$: contact-liquid phase.

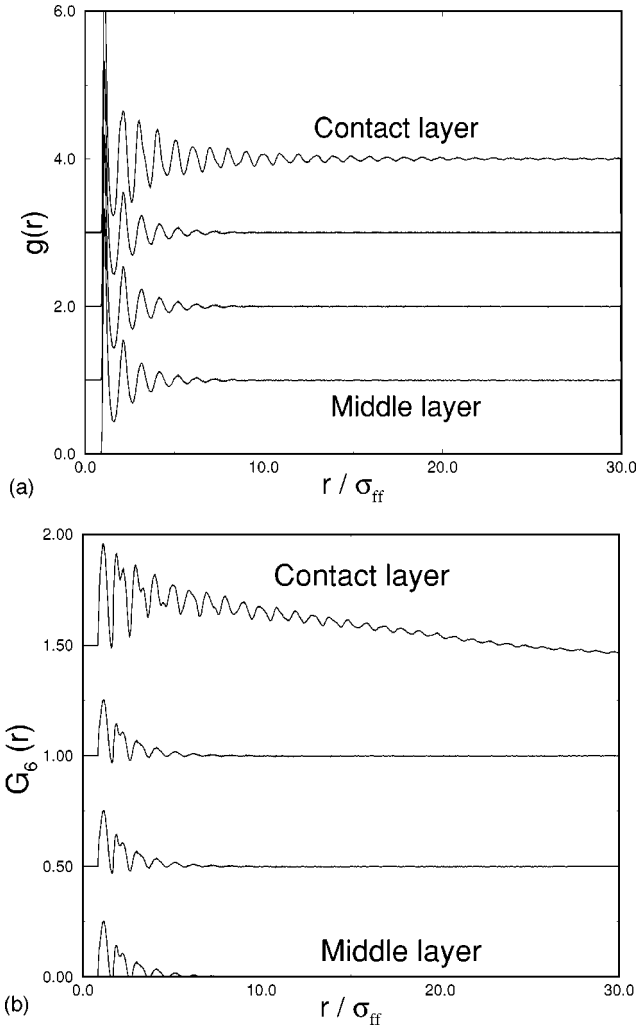

FIG. 9. The 2D in-plane (a) positional and (b) orientational pair correlation functions in the confined molecular layers for a LJ fluid in a slit-shaped pore of width $H=7.5\sigma_{ff}$ for $\alpha=2.16$, $T^*=0.85$: contact-hexatic phase.

while the contact-liquid phase consists of a liquidlike contact layer and crystalline inner layers (Fig. 8). The 2D $g(r)$ in the contact-hexatic phase is liquidlike in all the confined layers [Fig. 9(a)]; however, the orientational correlation function in the contact layer shows an algebraic $(1/r)$ decay while those in the inner layers show an exponential decay [Fig. 9(b)].

To illustrate the phase changes that occur on cooling, consider a slit-shaped pore of width $H=7.5\sigma_{ff}$ having an α value of 2.0. We start from the liquid phase at $T_{f,\mathrm{pore}}/T_{f,\mathrm{bulk}}=1.5$ and lower the temperature while maintaining a bulk pressure of 1 atm and ensuring that the system is at equilibrium. There will be a liquid-hexatic transition in the contact layers at $T_{f,\mathrm{pore}}/T_{f,\mathrm{bulk}}=1.35$. Upon further reducing the temperature to $T_{f,\mathrm{pore}}/T_{f,\mathrm{bulk}}=1.15$, the hexatic contact layers crystallize (while the inner layers remain fluidlike), leading to the formation of the contact-crystalline phase. At $T_{f,\mathrm{pore}}/T_{f,\mathrm{bulk}}=1.08$, the inner layers crystallize, and below this temperature the confined phase is comprised of stacked configurations of 2D hexagonal crystal.

The global phase diagram for a smaller pore width of $H=3\sigma_{ff}$ is shown in Fig. 10(a). For this choice of pore width there are no ''contact'' phases, as only two confined

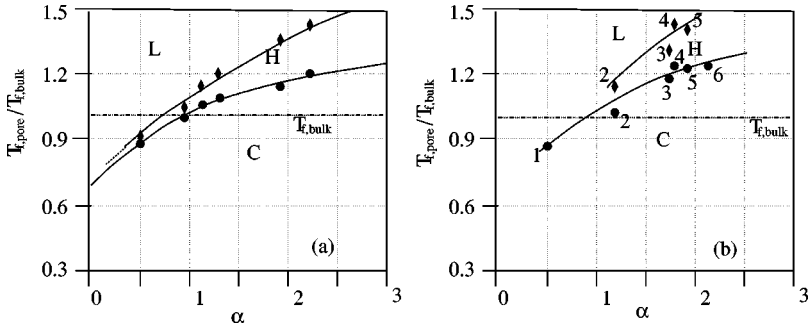

FIG. 10. (a) Global phase diagram of a fluid in a slit pore of width $H=3\sigma_{ff}$ from simulation. Three different phases are observed: liquid (L), hexatic (H), and crystalline (C). The dashed line represents an extrapolation of the phase boundaries based on MC simulations without free energy calculations. (b) Global phase diagram of a fluid in a slit pore of width $H\simeq 3\sigma_{ff}$ from experiment. The experiments are for various adsorbates confined within activated carbon fibers (ACF, mean pore width 1.4 nm): 1. H_2O (Ref. 13), 2. $C_6H_5NO_2$ (Ref. 14), 3. $C_6H_5NH_2$ (Ref. 15), 4. CH_3OH (Ref. 13), 5. CCl_4 (Refs. 11, 16), 6. C_6H_6 (Ref. 12).

molecular layers are present, both of which are contact layers. A similar phase diagram obtained from experimental results is shown in Fig. 10(b). The experimental results were taken from our previously published work and from the literature.[6,12–15,29] For each experimental system, the fluid–fluid interaction parameters were determined by fitting the Lennard-Jones potential to reproduce the bulk freezing point data (Table I). For methane, the Lennard-Jones parameters were chosen to reproduce the second virial coefficient data; these parameters gave a reasonable description of the freezing point of bulk methane. The pore wall potential parameters for activated carbon fiber were obtained from Steele.[29] For fluids with predominantly dispersive interaction (CCl_4, C_6H_{12}, and C_6H_6), the fluid-wall potential parameters were obtained from the fluid–fluid and wall–wall parameters, using Lorentz–Berthlot mixing rules. For dipolar fluids ($C_6H_5NO_2$, $C_6H_5NH_2$, and CH_3OH), the second virial coefficient data predicted by the LJ potentials in Table I was fitted to a Stockmayer potential,[41] and the ϵ_{ff} of the Stockmayer fluid was used in the Lorentz–Berthlot mixing rules to determine the fluid-wall parameters. This procedure was adopted as the dipole interactions of the polar fluids do not contribute to the fluid-wall potential, which is assumed to be purely dispersive (the polarizability of graphite and mica surfaces is small). For water, which has a hydrogen bonding character in addition to a large dipole moment, the ϵ_{ff} of the TIP4P potential[42] was used to determine the fluid-wall potential parameters. Again this assumes that the partial charges in the TIP4P potential do not contribute to the fluid-wall potential. The fluid–fluid parameters and the fluid-wall parameters for the experimental systems we have considered are given in Tables I, II, and III.

The phase boundaries shown in Figs. 10(a) and (b) are qualitatively similar. As α becomes smaller the temperature range where the hexatic phase is stable decreases. This is to be expected, since as α becomes small the fluid-wall interactions are relatively weaker, and the adsorbate no longer arranges itself into well defined quasi-two-dimensional layers. The crystal/hexatic boundary curves from simulation and experiment are in good agreement, within a few % for the freezing temperatures. The liquid/hexatic curves are qualitatively similar, but the experimental points show a larger scatter, with the agreement between simulation and experiment being within 12%.

All of the results shown here are for slit-shaped pores, for which well-defined phase transitions occur for all pore sizes. For cylindrical pores there will be two main differences in the freezing behavior. First, the freezing temperatures in a cylindrical pore are in general lower than for a slit pore of the same porous material and pore width.[43] This is because of the additional confinement in cylinders; it is clearly harder for the molecules to arrange themselves on the appropriate lattice points in a cylinder than in a slit geometry. Second, although freezing transitions occur in slit pores for all pore widths down to widths that accommodate just one layer of adsorbate, this is not the case for cylindrical pores. Both simulation[24] and experimental[24–27] studies have shown that for pore diameters below about $20\sigma_{ff}$ only partial freezing occurs, with a mixture of microcrystal and amorphous domains, while for still smaller pores even partial crystallization is not observed. Recent simulation and experimental studies suggest that this lower pore diameter below which no crystal domains occur is roughly $12\sigma_{ff}$ for silica materials.[24–27]

TABLE II. Fluid–fluid interaction parameters used to calculate the fluid-wall interactions.

Fluid	Model	Parameters	α
Simple fluids		σ_{ff}/nm, $\epsilon_{ff}/(k_BK)$	
C_6H_6	LJ	0.6, 401.0	2.18 (ACF)
C_6H_{12}	LJ	0.5, 412.0	2.22 (Mica)
CCl_4	LJ	0.514, 366.0	1.92 (ACF)
CH_4	LJ	0.381, 148.1	2.16 (ACF)
Dipolar fluids		σ_{ff}/nm, $\epsilon_{ff}/(k_BK)$, μ/Debye	
$C_6H_5NH_2$	Stockmayer	0.514, 358.0, 1.1	1.75 (ACF)
CH_3OH	Stockmayer	0.45, 176.0, 1.7	1.815 (ACF)
$C_6H_5NO_2$	Stockmayer	0.514, 212.0, 4.2	1.22 (ACF)
H-Bonding fluids			
H_2O	TIP4P	0.3154, 77.9, $q_O=-1.04$	0.51 (ACF)

TABLE III. Potential energy parameters for the pore walls.

Pore Wall Model	σ_{ww} / nm	$\epsilon_{ww}/(k_BK)$	ρ_w / nm^{-3}	Δ/ nm
Graphite (Ref. 29)	0.34	28.0	114	0.335
Mica (Ref. 9)	0.35	940.0	25.4	0.287

Recently more realistic models of porous glasses and activated carbon fibers have been developed,[44,45] that include dispersions in pore size, networking, connectivity and surface roughness found in the real porous materials. In the future, it is important to study the effect of the disorder of the porous matrix on the thermodynamic stability of the different confined phases.

This work was supported by grants from the National Science Foundation (Grant No. CTS-9908535) and the U.S.-Poland Maria Sklodowska-Curie Joint fund (Grant No. MEN/DOE-97-314). Supercomputer time was provided under a NSF/NRAC grant (MCA93S011).

[1] L. D. Gelb, K. E. Gubbins, R. Radhakrishnan, and M. Sliwinska-Bartkowiak, Rep. Prog. Phys. **62**, 1573 (1999).
[2] M. Miyahara and K. E. Gubbins, J. Chem. Phys. **106**, 2865 (1997).
[3] H. Dominguez, M. P. Allen, and R. Evans, Mol. Phys. **96**, 209 (1998).
[4] R. Radhakrishnan and K. E. Gubbins, Mol. Phys. **96**, 1249 (1999).
[5] M. A. Castro, S. M. Clarke, A. Inaba, and R. K. Thomas, J. Phys. Chem. B **101**, 8878 (1997).
[6] J. Klein and E. Kumacheva, Science **269**, 816 (1995).
[7] H. Hu, G. Carson, and S. Granick, Phys. Rev. Lett. **66**, 2758 (1991).
[8] S. Granick, Science **253**, 1374 (1991).
[9] S. T. Cui, P. T. Cummings, and H. D. Cochran, J. Chem. Phys. **114**, 7189 (2001).
[10] H. Christenson, Colloids Surf., A **123**, 355 (1997).
[11] K. Kaneko, A. Watanabe, T. Iiyama, R. Radhakrishnan, and K. E. Gubbins, J. Phys. Chem. **103**, 7061 (1999).
[12] A. Watanabe and K. Kaneko, Chem. Phys. Lett. **305**, 71 (1999).
[13] M. Sliwinska-Bartkowiak, G. Dudziak, R. Sikorski, R. Gras, K. E. Gubbins, and R. Radhakrishnan, Phys. Chem. Chem. Phys. **3**, 1179 (2001).
[14] R. Radhakrishnan, K. Gubbins, and M. Sliwinska-Bartkowiak, J. Chem. Phys. **112**, 11048 (2000).
[15] M. Sliwinska-Bartkowiak, R. Radhakrishnan, and K. E. Gubbins, Mol. Simul. **27**, 323 (2001).
[16] R. Radhakrishnan, K. E. Gubbins, and M. Sliwinska-Bartkowiak, preprint (2001).
[17] E. Molz, A. P. Y. Wong, M. H. W. Chan, and J. R. Beamish, Phys. Rev. B **48**, 5741 (1993).
[18] K. M. Unruh, T. E. Huber, and C. A. Huber, Phys. Rev. B **48**, 9021 (1993).
[19] K. Overloop and L. V. Gerven, J. Magn. Reson. **101**, 179 (1993).
[20] K. Morishige and K. Kawano, J. Chem. Phys. **110**, 4867 (1998).
[21] K. Morishige and K. Nabuoka, J. Chem. Phys. **107**, 6965 (1997).
[22] H. F. Booth and J. H. Strange, Mol. Phys. **93**, 263 (1998).
[23] M. Sliwinska-Bartkowiak, J. Gras, R. Sikorski, R. Radhakrishnan, L. D. Gelb, and K. E. Gubbins, Langmuir **15**, 6060 (1999).
[24] M. Sliwinska-Bartkowiak, G. Dudziak, R. Sikorski, R. Gras, R. Radhakrishnan, and K. E. Gubbins, J. Chem. Phys. **114**, 950 (2001).
[25] D. Morineau, G. Dosseh, C. Alba-Simionesco, and P. Llewellyn, Philos. Mag. B **79**, 1847 (1999).
[26] G. Dosseh, D. Morineau, and C. Alba-Simionesco, J. Phys. IV **10**, Pr7-99 (2000).
[27] D. Morineau, F. Casas, C. Alba-Simionesco, A. Grosman, M.-C. Bellisent-Funel, and N. Ratovélomanana, J. Phys. IV **10**, Pr7-95 (2000).
[28] W. A. Steele, Surf. Sci. **36**, 317 (1973).
[29] R. Radhakrishnan, K. Gubbins, A. Watanabe, and K. Kaneko, J. Chem. Phys. **111**, 9058 (1999).
[30] R. M. Lynden-Bell, J. S. van Duijneveldt, and D. Frenkel, Mol. Phys. **80**, 801 (1993).
[31] P. M. Chaikin and T. C. Lubinski, *Principles of Condensed Matter Physics* (Cambridge University Press, Cambridge, 1995).
[32] N. D. Mermin and H. Wagner, Phys. Rev. Lett. **17**, 1133 (1966).
[33] D. R. Nelson and B. I. Halperin, Phys. Rev. B **19**, 2457 (1979).
[34] J. M. Kosterlitz and D. J. Thouless, J. Phys. C **6**, 1181 (1973).
[35] B. K. Peterson and K. E. Gubbins, Mol. Phys. **62**, 215 (1987).
[36] D. A. Kofke, J. Chem. Phys. **98**, 4149 (1993).
[37] R. Agrawal and D. A. Kofke, Mol. Phys. **85**, 43 (1995).
[38] For strongly attractive pores, there exists a possibility of hexatic transitions in the layers other than the contact layers, although such transitions were not observed in our simulations. Since these are subtle phase transitions, they have a strong dependence on system size. Therefore their occurrence in the infinite system cannot be ruled out based on our calculations.
[39] For modeling the potential due to mica surfaces in the surface force apparatus (SFA), Cui *et al.* (Ref. 9) fitted the parameters of the 10-4-3 Steele potential [Eq. (2)], to reproduce the surface energy of 220 mJ/m^2 reported in experiments (Ref. 8; see Table III). By using the 10-4-3 potential, Cui *et al.* (Ref. 9) assumed that the wall-potential due to mica surfaces is purely dispersive. However, as reported by Tsujimichi *et al.* (Ref. 40) in a atomic force microscopy (AFM) study of cleaved mica surfaces, there is a distribution of K^+ ions in a background of SiO_4^{4-} and AlO_4^{5-} ions, so that induction forces may make a significant contribution.
[40] K. Tsujimichi, H. Tamura, A. Hirotani, M. Kubo, M. Komiyama, and A. Miyamoto, J. Phys. Chem. B **101**, 4260 (1997).
[41] J. O. Hirshfelder, C. F. Curtiss, and B. Bird, *Molecular Theory of Gases and Liquids* (Wiley, New York, 1964).
[42] W. L. Jorgensen, J. Chandrasekhar, and D. Madura, J. Chem. Phys. **79**, 926 (1983).
[43] M. Maddox and K. E. Gubbins, J. Chem. Phys. **107**, 9659 (1997).
[44] L. D. Gelb and K. E. Gubbins, Langmuir **14**, 2097 (1998).
[45] K. Thomson and K. Gubbins, Langmuir **16**, 5761 (2000).